Physical images of relative timescales in coevolution dynamics

Chao-Ran Cai,[1,2,*] Na-Na Liu,[1] Xin Chang,[1,3] and Xu-Sheng Liu[4]
[1]*School of Physics, Northwest University, Xi'an 710127, China*
[2]*Shaanxi Key Laboratory for Theoretical Physics Frontiers, Xi'an 710127, China*
[3]*Institute of Modern Physics, Northwest University, Xi'an 710127, China*
[4]*School of Science, East China University of Technology, Nanchang, Jiangxi 330013, China*

(Received 11 July 2023; accepted 19 September 2023; published 27 September 2023)

In this paper, we propose three physical images, namely, asymmetric external inputs, discretization of the low rate region, and secondary outbreak, to understand the mystery of the relative timescales in the coevolution dynamics on multiplex networks. We carry out our analysis on an irreversible information-epidemic coevolution dynamics. In this dynamics, we found five kinds of anomalous behaviors, which are that with the increase of relative information processing speed, the final epidemic size may be monotonically increasing, monotonically decreasing, first decreasing and then increasing, first increasing and then decreasing but increasing again, and suddenly increasing with large fluctuation. Such complex behavior can be fully explained by our three physical images. Moreover, these five behaviors may transform into one another, which is far more complex than cyclic dynamics. Of course, our physical images easily provide an explanation for the results of cyclic coevolution dynamics. Since our discussion does not rely on specific dynamics and networks, our research may readily be extended to a broader field, rather than the network epidemiology in this paper.

DOI: 10.1103/PhysRevResearch.5.033220

I. INTRODUCTION

With the maturity and reliability of the single epidemic spreading model on networks [1–7], more and more researchers have paid attention to the coupled evolution of multiple dynamic models in the past decade [8–14], including coevolution of two diseases [15–21], coevolution of information and epidemic [22–24], and coevolution of resource and epidemic [25–28]. In the real world, disease, behavior, and information often coevolve through strong interactions [29]. For example, susceptibility to malaria is enhanced in HIV infected patients [30]; disease related information generated through first hand observation and word of mouth transmission can suppress the spread of the corresponding epidemic disease [31]. For some special cases, such as multiple diseases spreading in the same way, one can study on a single layer network [32–34]. In most cases, however, it is more convincing to use a multiplex network or multilayer network. Compared with the universality of the concept of multilayer networks [35–39], the multiplex network, as a special case of the multilayer network, emphasizes that different layers have the same set of nodes [40–43]. Most work on the coevolution of information and disease uses multiplex networks [44–47], because individuals can both be infected and be aware of information.

So far, a great deal of effort has been devoted to the study of information-epidemic dynamics on multiplex networks and a number of important results have been achieved [22–24,44–54]. For example, Granell *et al.* extended the microscopic Markov chain approach to the information-epidemic model and found the emergence of a metacritical point from which the transmission of information can control the epidemic threshold [22]. Moreover, the metacritical point disappears if one considers that the mass media can spread awareness [23]. In Ref. [23], a surprising finding is that the results always satisfy a specific inverse linear expression when fitting the threshold results. Inspired by this, Chang *et al.* gave the theoretical relationship between the epidemic threshold on the decoupled epidemic layer network and that on the multiplex network [45]. Huang *et al.* modified the dynamic behavior of aware individuals and found that such heterogeneous interactions can induce hybrid phase transitions with the coexistence of both continuous and discontinuous phase transitions [44]. Wang *et al.* found that there is an optimal information transmission rate that minimizes the disease spreading in the SIR framework [49]. Considering the effect of social reinforcement, many researchers have reached some interesting results by introducing 2-simplices into the information layer. For example, the introduction of 2-simplices can increase the epidemic threshold [46–48]. Multiple susceptibility peaks emerge in the susceptibility of the epidemic layer under the combined effect of simplicial complexes and self-awareness [47]. The differences between individuals for acceptance of information and self-protection measures have important impacts on dynamic behavior [48].

More recently, Wang *et al.* introduced the concept of the relative timescales into information-epidemic dynamics and they found that faster information dissemination

*ccr@nwu.edu.cn

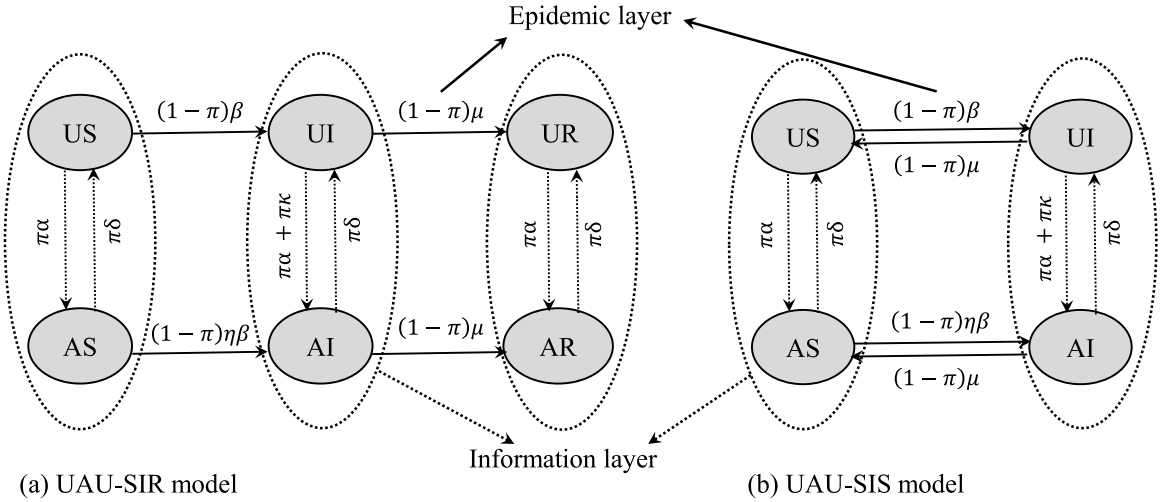

FIG. 1. Schematic illustrations showing the states of the individuals for the UAU-SIR model in (a) and the UAU-SIS model in (b) on a multiplex network and the associated transition rates between states. For the UAU-SIR model, individuals can be in six possible states: Unaware and susceptible (US), aware and susceptible (AS), unaware and infected (UI), aware and infected (AI), unaware and recovered (UR), and aware and recovered (AR). For UAU-SIS model, individuals can only be in the first four states. The dotted arrows within the dotted ellipses represent state transitions occurring within the information layer, while the solid arrows represent state transitions occurring within the epidemic layer.

does not always better mitigate the epidemic spreading which contradicts our intuition [50]. Meanwhile, in another information-epidemic model, Ventura da Silva *et al.* found that higher self-awareness can also lead to counterintuitive results with higher epidemic prevalence when information spreads much faster than disease [51]. To rule out the complexity of the model, Velásquez-Rojas *et al.* used the simplest UAU-SIS model to make it clear once again that the epidemic prevalence increases with the speed of information processing [52]. In addition, the authors in Ref. [52] provided analytical solutions of the mean field theory to understand these phenomena, but as the authors state in the conclusion, the counterintuitive phenomena are not fully explored and understood. It is worth mentioning that Ventura da Silva *et al.* also found a similar phenomenon on the coevolution dynamics of two diseases, suggesting that the counterintuitive phenomenon may be an intrinsic feature of such coevolution dynamics [20]. However, the lack of a clear physical image for understanding the phenomenon has also hindered its flexible application or prevention, as well as its extension to other models. Meanwhile, it is unclear whether a similar phenomenon would occur in irreversible models, such as the SIR type model.

In this paper, we present three physical images, which do not depend on specific dynamical models, to understand the counterintuitive phenomena of the relative timescales in the coevolution dynamics on multiplex networks. We also find counterintuitive phenomena related to timescales in irreversible dynamics (UAU-SIR model), which are much more complex and difficult to understand than cyclic dynamics. Regardless of cyclic dynamics or irreversible dynamics, all phenomena can be explained by the physical images presented in this paper.

The rest of the paper is organized as follows. In Sec. II, the information-epidemic dynamics used in this paper is described in detail. In Sec. III, we present three physical images related to timescales. In Sec. IV, we give a large number of simulation results and numerical analysis results related to the relative timescales and we explained these results in detail using the physical images of Sec. III. Finally, we summarize our results in this work in Sec. V.

II. MODEL

In this paper, we consider two kinds of information-epidemic coevolution models on multiplex networks, namely, the UAU-SIR model [Fig. 1(a)] and the UAU-SIS model [Fig. 1(b)]. For the former, the process of the epidemic layer is irreversible, while, for the latter, it is reversible (cyclic). Nodes in different layers represent the same individuals, but they may be connected differently in the two layers.

In the information layer, the population is divided into two classes, unaware (U) and aware (A). Links between U and A transmit the epidemic related information (i.e., the unaware individual receives the information) with a rate α. Aware individuals become unaware again with rate δ. Furthermore, an unaware individual spontaneously becomes aware (self-awareness) with rate κ when it is infected.

In the epidemic layer, we implement the SIR (or SIS) epidemic dynamics in the following way. When a susceptible (S) individual is in the U state or the A state, the susceptible individual becomes infected by contact with infected (I) individuals at the rate β or $\eta\beta$ multiplying the number of S-I edges. Here, $\eta \in [0, 1]$ denotes the strength of the reduction in infection rates after an aware individual's actions, such as wearing a face mask. Infected individuals get cured to be recovered (R) individuals (or susceptible individuals again) with rate μ. The recovered individuals are not infected and do not have the ability to infect others.

Finally, the relative timescales of the models are controlled by introducing a parameter π [51,52], where $\pi \in [0, 1]$. Specifically, we multiply the transformation rates of the information layer and the epidemic layer by π and $1-\pi$,

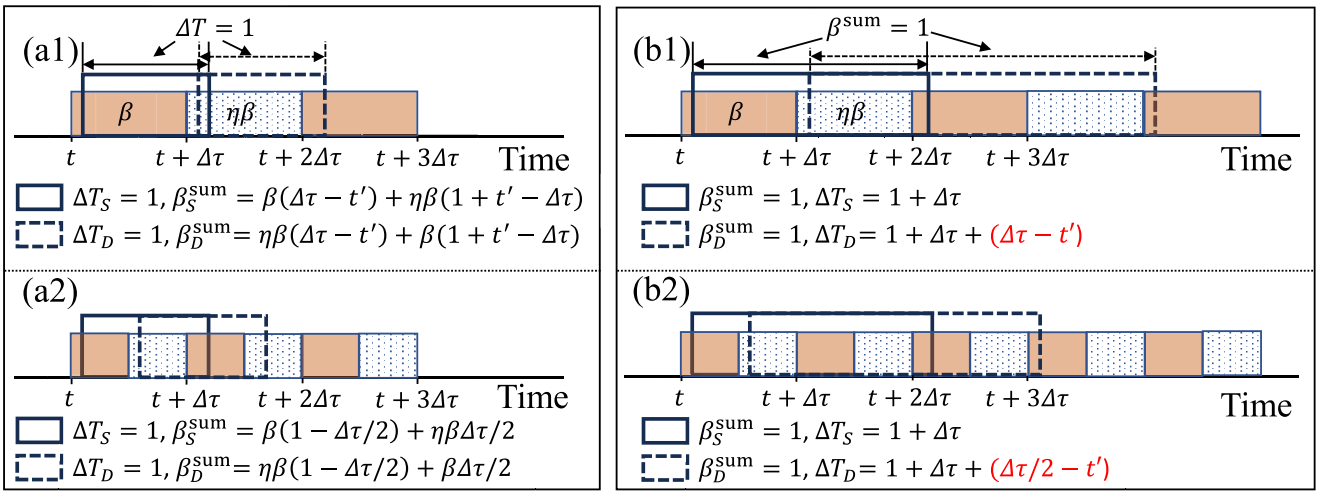

FIG. 2. Schematic illustration of discretization of the low rate region. ΔT_S and ΔT_D are the durations of solid and dashed windows, respectively. $\beta_S^{\rm sum}$ and $\beta_D^{\rm sum}$ are the accumulation rates of solid and dashed windows, respectively. The beginning moment of the solid window is in the high rate region with the value $t + t'$, where $t' \in [0, \Delta\tau)$ in panels (a1) and (b1) and $t' \in [0, \Delta\tau/2)$ in panels (a2) and (b2). The beginning moment of the corresponding dashed window is in the low rate region and its value is $t + \Delta\tau + t'$ in panels (a1) and (b1) and $t + \Delta\tau/2 + t'$ in panels (a2) and (b2). (a1),(a2) The average rate generated per unit time is analyzed by the fixed window duration $\Delta T = 1$. Because $\beta_S^{\rm sum} + \beta_D^{\rm sum}$ is independent of t', the average rate generated per unit time is $\frac{1}{2}(\beta_S^{\rm sum} + \beta_D^{\rm sum}) = 0.5(\beta + \eta\beta)$ for both panels (a1) and (a2), which means that discretization of the low rate region does not affect the average rate generated per unit time. (b1),(b2) The average time required per unit rate is analyzed by a fixed accumulation rate $\beta^{\rm sum} = 1$. Although ΔT_S of panels (b1) and (b2) are equal, ΔT_D of panel (b2) is greater than ΔT_D of panel (b1), so discretization of the low rate region reduces the average time required per unit rate. The red terms in panels (b1) and (b2) represent the time it takes for the dashed window to go through the first low rate region, which is the source of the reduction in the average time required per unit rate. Parameters: $\beta = 1$, $\eta = 0.0$, and $\Delta\tau = 0.9$.

respectively. Thus an increase in π represents an increase in the speed of information processing.

We use two capital letters to denote the composite state of an individual, the first denoting the information state and the second denoting the epidemic state. For the UAU-SIR model, individuals can be in six possible states: Unaware and susceptible (US), aware and susceptible (AS), unaware and infected (UI), aware and infected (AI), unaware and recovered (UR), and aware and recovered (AR). For the UAU-SIS model, individuals can only be in the first four states. The transitions among all of the above states are shown in Fig. 1.

III. PHYSICAL IMAGES

We focus on the effect of the increased speed of information processing on the epidemic layer. As π increases, two immediate and obvious effects occur. One is that the information layer reaches its steady state faster and the other is that the individual changes its state more frequently in the information layer. The latter results in the low rate region (suppression effect) being more discrete in time in the epidemic layer.

A. Discretization of the low rate region

In Fig. 2, we first analyze the property that the low rate region (the region of $\eta\beta$) of the epidemic layer tends to be discrete, where panels (a2) and (b2) are more discretized than panels (a1) and (b1). The duration interval of the low rate area (while keeping the ratio of low to high rate constant), as the only control variable in Figs. 2 and 3, represents the degree of discretization.

In general, the higher the average infection rate per unit time, the greater the epidemic size in the epidemic layer will be. In Figs. 2(a1) and 2(a2), we analyze the average rate generated per unit time with a fixed window duration $\Delta T = 1$. We define $\beta_S^{\rm sum}$ and $\beta_D^{\rm sum}$ as the accumulation rates

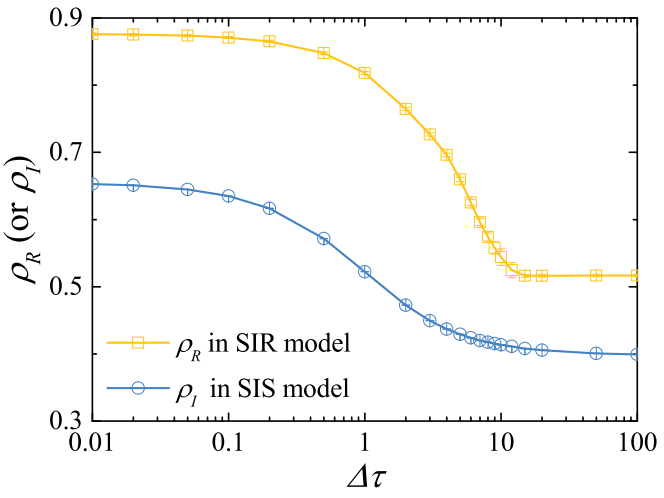

FIG. 3. Discretization of the low rate region for SIR and SIS models. The network is the Erdős-Rényi network with network size $N = 10^5$ and average degree $\langle k \rangle = 10$. 37.7% of the individuals in the system are labeled, the infection rate of the labeled individuals is reduced to $\eta\beta$, and the labels are randomly selected again after $\Delta\tau$ intervals. The simulation results are obtained by averaging over 100 independent runs. Parameters: $\beta = 0.5$, $\mu = 1.0$, $\eta = 0.0$, and $\rho_I(0) = 0.01$.

of solid and dashed windows, respectively. The beginning moment of the solid window is in the high rate region (the region of β) with the value $t+t'$, where $t' \in [0, \Delta\tau)$ in Fig. 2(a1) and $t' \in [0, \Delta\tau/2)$ in Fig. 2(a2). The beginning moment of the corresponding dashed window is in the low rate region and its value is $t+\Delta\tau+t'$ in Fig. 2(a1) and $t+\Delta\tau/2+t'$ in Fig. 2(a2). The average rates in Fig. 2(a1) and Fig. 2(a2) can be calculated by $\frac{1}{2\Delta\tau}\int_0^{\Delta\tau}(\beta_S^{\text{sum}}+\beta_D^{\text{sum}})dt'$ and $\frac{1}{\Delta\tau}\int_0^{\frac{\Delta\tau}{2}}(\beta_S^{\text{sum}}+\beta_D^{\text{sum}})dt'$. Notice that, for any given solid window in either Fig. 2(a1) or Fig. 2(a2), we can always find a dashed window so that the rate sum of the two windows is $\beta_S^{\text{sum}}+\beta_D^{\text{sum}}=\beta+\eta\beta$. Therefore, the average rate generated per unit time is always equal to $0.5(\beta+\eta\beta)$, which is independent of the discretization of the low rate region. In the above conventional way of thinking, one would assume that the relative timescales do not affect the epidemic size, which is why the counterintuitive phenomenon (faster transmission of information increases the epidemic size) mentioned in the Introduction was not understood.

In contrast to the common thinking, we next take into account the average time it takes to accumulate the unit rate $\beta^{\text{sum}}=1$; see Figs. 2(b1) and 2(b2). We define ΔT_S and ΔT_D as the durations of solid and dashed windows, respectively. The beginning moment of the solid window is in the high rate region with the value $t+t'$, where $t' \in [0, \Delta\tau)$ in Fig. 2(b1) and $t' \in [0, \Delta\tau/2)$ in Fig. 2(b2). The beginning moment of the corresponding dashed window is in the low rate region and its value is $t+\Delta\tau+t'$ in Fig. 2(b1) and $t+\Delta\tau/2+t'$ in Fig. 2(b2). For the solid window, it is shown that ΔT_S in Fig. 2(b1) is equal to ΔT_S in Fig. 2(b2). However, ΔT_D in Fig. 2(b2) is shorter than ΔT_D in Fig. 2(b1). Thus discretization of the low rate region can reduce the average time required per unit rate. The red terms in ΔT_D of Fig. 2(b1) and Fig. 2(b2) represent the time it takes for the dashed window to pass through the first low rate region, which is the source of the decrease in the average time required per unit rate.

To sum up the above two aspects, although the discretization of the suppression effect will not affect the average rate generated per unit time, it will shorten the average time required per unit rate, thus making the disease easier to spread. Some notes are as follows. First, the analysis of the physical image applies not only to the suppression effect but also to the promotion effect (see Sec. IV C), because they are both composed of low rate regions and high rate regions. Thus we call the physical image the discretization of low rate region. Second, the low and high rate regions in Fig. 2 are proportioned equally for illustrative purposes only and our analysis is robust to any proportion. Last but not least, the physical image in this subsection does not include any specific dynamic model, which means that the image works on both irreversible and cyclic dynamics.

To observe more directly the influence of discretization of the low rate region on the dynamics, we plot Fig. 3 for classical SIR and SIS models [55]. In Fig. 3, 37.7% of the individuals were randomly selected as low infection rate and were randomly reselected after each time interval $\Delta\tau$. Figure 3 shows that the prevalence of both the SIR model and the SIS model decreases with the increase of $\Delta\tau$, which directly indicates that the higher the degree of discretization (the smaller the $\Delta\tau$), the larger the final epidemic size.

In addition, it can be seen from Fig. 3 that, when $\Delta\tau$ is small enough, the prevalence tends to a maximum value, because the degree of discretization is uniform enough. For the SIR model, when $\Delta\tau$ is large enough, the prevalence is fixed at a minimum value, because $\Delta\tau$ is already longer than the propagation time of the system.

B. Asymmetric external inputs

Now, we analyze the property that the information layer reaches its steady state faster. The parameters of the information layer are divided into two categories: α and δ regulate the intensity of intralayer spreading (information prevalence); $\rho_A(0)$ and κ regulate the number of external inputs to aware individuals [47].

Here, there are two kinds of asymmetry between intensity of intralayer diffusion and the number of external inputs. For $\rho_A(0)$, there is an asymmetry between the continuous generation of aware individuals within the layer and the one-time external input of individuals. For κ, there may be an asymmetry in the multiplied magnification coefficients between the parameters (κ, α, and δ).

For the UAU-SIR model, the number of aware individuals generated by self-awareness is limited and, more importantly, these individuals can only indirectly suppress the epidemic layer through the information spreading on the information layer, so the effect of κ in the UAU-SIR model is very weak. In the information layer, the information prevalence ρ_A may be different from $\rho_A(0)$, resulting in different inhibitory effects on the epidemic layer. We know that the information layer reaches its steady state faster as π increases. Therefore, if ρ_A is greater than $\rho_A(0)$, the system will reach higher suppression more quickly as π increases, while, if $\rho_A < \rho_A(0)$, the system will achieve lower inhibitory effect faster.

For the UAU-SIS model, the effect of $\rho_A(0)$ is negligible because the epidemic layer reaches its steady state. Meanwhile, the external input of the information layer is symmetric with the propagation intensity within the layer, that is, α, δ, and κ are multiplied by π at the same time. Therefore, we do not need to consider the effect of asymmetric external input in the UAU-SIS model. However, if the coefficient before κ is not π, this effect needs to be considered.

C. Secondary outbreak

For irreversible dynamics, secondary outbreak is possible; see Fig. 4. From Fig. 4(a), we can clearly see the first outbreak at $\rho_R \approx 0.43$ and the second outbreak at $\rho_R \approx 0.52$. In Fig. 4(b), ρ_I reaches the first peak at $t \approx 3.6$ and, after this point, the effective reproduction number is less than 1 and ρ_I gradually decreases. Meanwhile, Fig. 4(c) shows that ρ_A decreases monotonically with time. The infection rate in many susceptible individuals returns to β from $\eta\beta$, which increases the effective reproduction number. When the effective reproduction number is greater than 1 again, a secondary outbreak occurs. Since the effective reproduction number is also related to the network structure of the remaining susceptible individuals, the secondary outbreak cannot be guaranteed even when

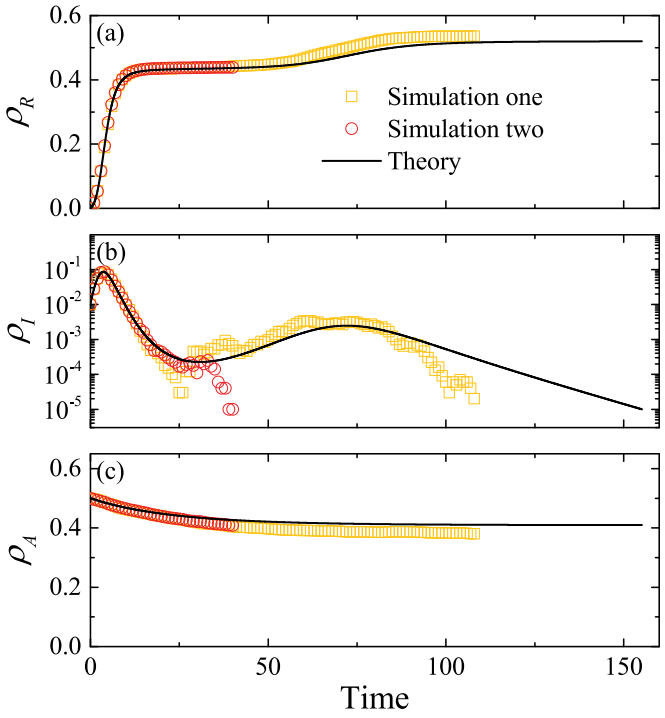

FIG. 4. Time series for the UAU-SIR model. The lines are obtained from Eq. (A1), while scatters are obtained by Monte Carlo simulations. The multiplex network consists of two independent Erdős-Rényi networks with network size $N = 10^5$, both of which have an average degree $\langle k \rangle = 10$. Parameters: $N = 10^5$, $\beta = 0.5$, $\mu = 1.0$, $\alpha = 0.1$, $\delta = 0.6$, $\kappa = 0.0$, $\eta = 0.0$, $\pi = 0.08$, $\rho_A(0) = 0.5$, and $\rho_I(0) = 0.01$.

simulated under the same parameters, which is the source of fluctuations. Figure 4 shows the results of two simulations, where the square produces a secondary outbreak but the circle does not.

Therefore, there are two necessary conditions for a secondary outbreak. On the one hand, after ρ_I reaches its first peak, the proportion of aware individuals is gradually reduced to release more protected individuals, as shown in Fig. 4(c). On the other hand, the prevalence of the first outbreak must not be too high to ensure that there are enough remaining susceptible individuals to participate in the second outbreak. This also creates a network size requirement and we have not seen a secondary outbreak when running Monte Carlo simulations for a population with $N = 1000$ (not shown here).

IV. RESULTS AND DISCUSSION

In this section, we use two independent Erdős-Rényi network layers to build a multiplex network. The average degree of both layers is fixed at 10 and the network size is fixed at $N = 10^5$. Our key concern is how the final epidemic size ρ_R (or ρ_I) changes over the relative timescales in the UAU-SIR (or UAU-SIS) model. For the UAU-SIR model, we give the theoretical analysis and simulation procedure in Appendix A and Appendix B, respectively.

A. Results for the UAU-SIR model

In Fig. 5, we plot the final epidemic size ρ_R as a function of the relative timescales π for different awareness rate α and initial seeds $\rho_A(0)$. It can be seen from Fig. 5 that ρ_R presents five different behaviors as the relative timescales π increase, namely, monotonically increasing (MI), monotonically decreasing (MD), first decreasing and then increasing (DI), first increasing and then decreasing but increasing again (IDI), and suddenly increasing with large fluctuation (IF).

As can be seen from Fig. 5(a), the behavior of the curve $\rho_R(\pi)$ transitions from DI to MI and then to IF with the increase of $\rho_A(0)$ [56]. From Fig. 5(b), the behavior of $\rho_R(\pi)$ changes from MI to IDI and then to MD with the increase of α when $\rho_A(0) = 0.1$. But when $\rho_A(0)$ increases to 0.5, Fig. 5(c) shows that the behavior of $\rho_R(\pi)$ transitions from IF to DI and then to MD as α increases, which is quite different from Fig. 5(b). Such complexity means that there are several physical mechanisms acting on these phenomena, not just one. We will analyze all the phenomena in detail in Sec. IV B by using the physical images in Sec. III.

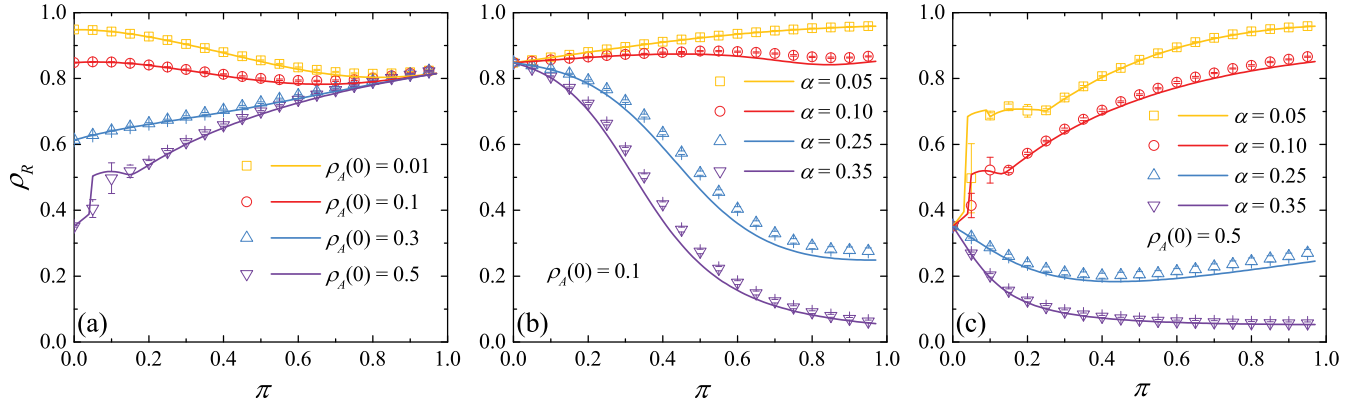

FIG. 5. Final epidemic size ρ_R as a function of the relative timescales π for different awareness rate α and initial seeds $\rho_A(0)$ in the information layer. The lines are obtained from Eqs. (A1) and (A2), while scatters are obtained by Monte Carlo simulations, which are averages over 100 independent runs. The multiplex network consists of two independent Erdős-Rényi networks with network size $N = 10^5$, both of which have an average degree $\langle k \rangle = 10$. Parameters: $\beta = 0.5$, $\mu = 1.0$, $\delta = 0.6$, $\eta = 0.0$, and $\rho_I(0) = 0.01$; (a) $\alpha = 0.1$ and $\kappa = 5.0$; (b) $\kappa = 0.0$ and $\rho_A(0) = 0.1$; (c) $\kappa = 0.0$ and $\rho_A(0) = 0.5$.

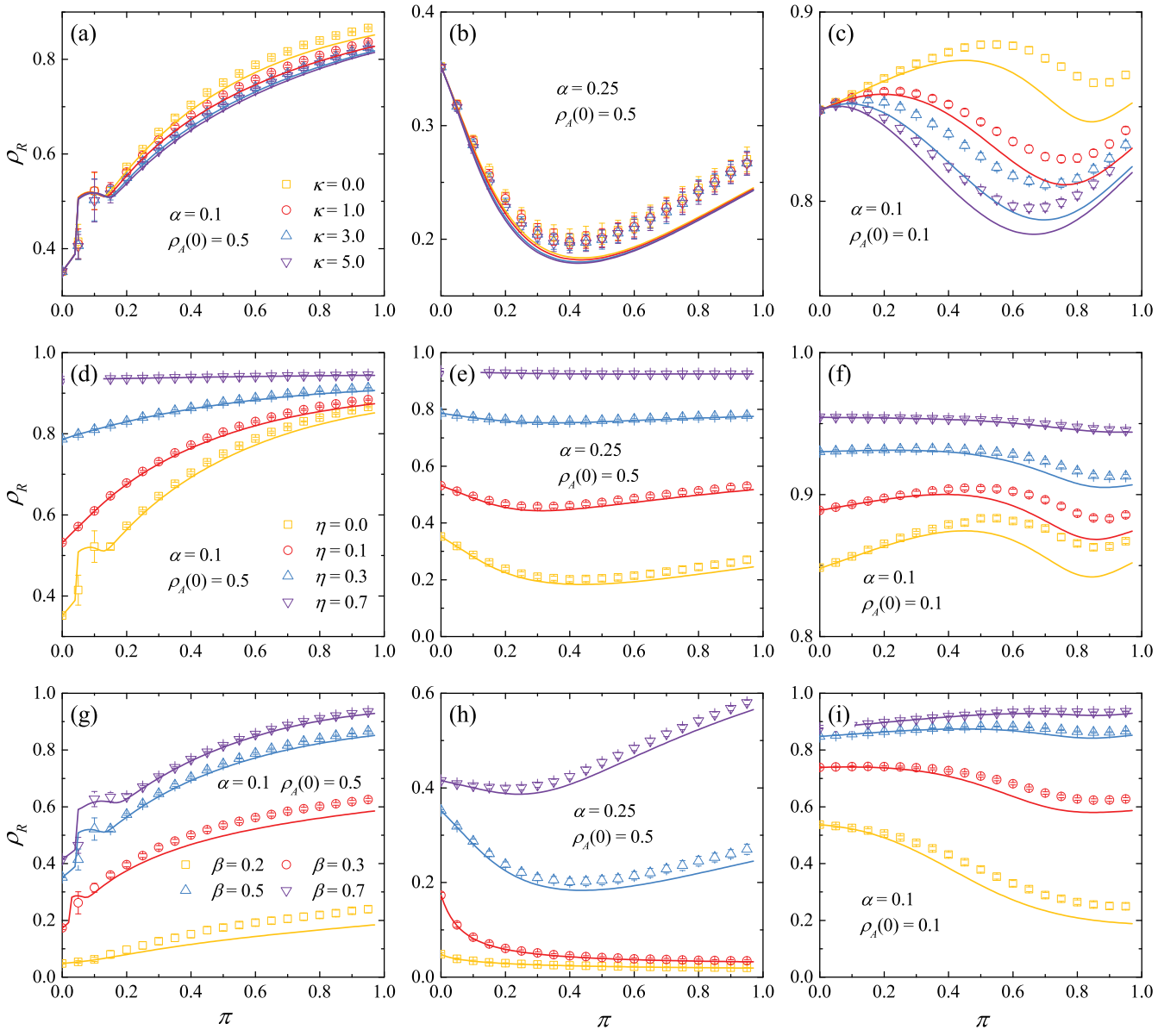

FIG. 6. Final epidemic size ρ_R as a function of the relative timescales π for different η, κ, and β. The lines are obtained from Eqs. (A1) and (A2), while scatters are obtained by Monte Carlo simulations, which are averages over 100 independent runs. The network is the same as in Fig. 5. Parameters: $\mu = 1.0$, $\delta = 0.6$, and $\rho_I(0) = 0.01$. [(a)–(c)] $\beta = 0.5$, $\eta = 0.0$, and different shapes (or colors) represent different κ; [(d)–(f)] $\beta = 0.5$, $\kappa = 0.0$, and different shapes (or colors) represent different η; [(g)–(i)] $\kappa = 0.0$, $\eta = 0.0$, and different shapes (or colors) represent different β.

To further investigate the influence of the epidemic layer parameters on these phenomena, in Fig. 6, we plot the effects of changing the η, κ, and β parameters on the three nonmonotonic phenomena mentioned above. Specifically, the left column of Fig. 6 shows the change of IF, the middle column shows the change of DI, and the right column shows the change of IDI.

It can be seen from Figs. 6(a)–6(c) that the change of κ has little quantitative or even no qualitative influence on the behavior of the curve, especially when $\rho_A(0)$ is large. Due to the irreversibility of the dynamics on the epidemic layer, the number of aware individuals generated by self-awareness is limited and, more importantly, these individuals can only indirectly suppress the epidemic layer through the information spreading on the information layer, so the effect of κ in the UAU-SIR model is very weak. For the larger η in Figs. 6(d)–6(f), ρ_R does not change much with π because the information layer has a weak influence on the epidemic layer. For smaller η, Figs. 6(e) and 6(f) cannot see the qualitative influence of η on the curve behavior, while the behavior of IF in Fig. 6(d) disappears with the increase of η. Figures 6(g)–6(i) show that the three nonmonotonic curves become monotonic with the decrease of β.

Apart from these complicated phenomena, there are some general phenomena in Figs. 5 and 6. Figure 5 shows that ρ_R decreases with the increase of $\rho_A(0)$ or α, because the increase of $\rho_A(0)$ or α leads to an increase in the number of aware individuals. Meanwhile, in Figs. 6(a)–6(c), ρ_R decreases as

κ increases for the same reason. The increase of η means that the suppression effect of the information layer on the epidemic layer is weakened, which leads to more susceptible individuals being infected, so it can be seen in Figs. 6(d)–6(f) that ρ_R increases with η. Figures 6(g)–6(i) show that ρ_R decreases as β increases.

B. Discussion based on physical images for the UAU-SIR model

For the sake of simplicity, we refer to the physical images in Sec. III B, Sec. III A, and Sec. III C as *image 1*, *image 2*, and *image 3*, respectively.

If $\rho_A > \rho_A(0)$, *image 1* tells us that ρ_R decreases as π increases, while *image 2* does the opposite. Therefore, there is a competition between the two physical images. When *image 1* is fully dominant for any π, the curve will behave as MD, while *image 2* is completely dominant and the curve will behave as MI. If neither is fully dominant for any π, the curve will behave as a complex nonmonotonic behavior. For *image 1*, its effect increases as the difference between ρ_A and $\rho_A(0)$ increases. Meanwhile, the effect of *image 1* will also reach saturation when π is relatively large, because the time for the information layer to reach its steady state will reach the limit. As can be seen from the slope of the curve in Fig. 3, with the increase of π from small to large ($\Delta\tau$ from large to small), the increase rate of the effect of *image 2* will gradually decrease. The above three points make IDI and DI qualitatively understandable.

For Fig. 5(a), *image 1* dominates when π is small, but when π is large, *image 2* dominates as the effect of *image 1* gradually decreases and reaches saturation. Thus the curve shows the behavior of DI. As $\rho_A(0)$ increases, *image 1* changes to match *image 2* and the disappearance of the competition causes the curve to transition to MI. It should be noted that, at this point, the first condition of *image 3* has been triggered, which is the increase of the infection rate of susceptible individuals. With the further increase of $\rho_A(0)$, the gradual increase of the remaining susceptible individuals finally triggers the second necessary condition for *image 3*, so that the curve shows the behavior of IF.

In Figs. 5(b) and 5(c), we set $\kappa = 0$ to facilitate obtaining the information prevalence ρ_A through theoretical calculation; see Appendix C for details. We know that ρ_A increases as α increases, which makes *image 1* transition from $\rho_A < \rho_A(0)$ to $\rho_A > \rho_A(0)$. So, as α increases, the curves generally transition from increasing to decreasing. For the circle in Fig. 5(b), the lower $\rho_A(0)$ [compared to Fig. 5(c)] weakens the effect of *image 1*, which gives *image 2* an advantage in the competition when π is small. However, the increase in the effect of *image 2* decreases as π increases, making *image 1* dominant. When π is large, the increase in the effect of *image 1* also gradually decreases and reaches saturation, allowing *image 2* to regain dominance. These are the reasons why the circle curve with $\alpha = 0.1$ in Fig. 5(b) produces the behavior of IDI. The effect of *image 1* is strong when ρ_A is much larger than $\rho_A(0)$. Comparing the triangle curves of Fig. 5(b) and 5(c), the difference between ρ_A and $\rho_A(0)$ is different, which determines whether *image 1* can always dominate. In Fig. 5(c), we increase $\rho_A(0)$ to 0.5, at which point two necessary conditions for *image 3* are triggered. We see that, as α decreases, the behavior of IF becomes more pronounced, as the protected individuals are released more and faster.

For Figs. 6(a)–6(c), due to the irreversibility of the epidemic layer, self-awareness has little effect on the behavior of the curve, which is mentioned in Sec. IV. Meanwhile, there is no qualitative change in curve behavior of Figs. 6(e) and 6(f).

For Fig. 6(d), an increase in η leads not only to a decrease in $\beta - \eta\beta$ (the increment of infection rate) as the susceptible individuals lose protection, but also to a decrease in the number of remaining susceptible individuals. The latter is the main reason for the disappearance of IF based on the analysis of *image 3*. In Figs. 6(g)–6(i), a decrease in β also results in a decrease in the value of $\beta - \eta\beta$. For Fig. 6(g), although the number of remaining susceptible individuals does not decrease, the decrease in $\beta - \eta\beta$ affects the range of the behavior of IF, causing the behavior to gradually disappear. For Figs. 6(g)–6(i), the decrease in $\beta - \eta\beta$ reduces the difference between the high- and the low-rate region in *image 2*, resulting in its weakening and the dominance of *image 1*. By numerical calculation of Eqs. (C1) and (C2), we know that $\rho_A(0)$ is greater than ρ_A in Fig. 6(g) and $\rho_A(0) < \rho_A$ in Fig. 6(h) and Fig. 6(i). Thus, for a small β (e.g., $\beta = 0.2$), the curve of Fig. 6(g) shows the behavior of MI, while the curves in Fig. 6(h) and in Fig. 6(i) show the behavior of MD.

C. Discussion based on physical images for the UAU-SIS model

Our physical image analysis also applies to the UAU-SIS model. Since the cyclic model reaches its dynamic equilibrium, there is no secondary outbreak. Meanwhile, the external input of the information layer is symmetric with the propagation intensity within the layer; that is, α, δ, and κ are multiplied by π at the same time. Therefore, in the UAU-SIS model, only *image 2* is at work and we mainly see that the epidemic prevalence ρ_I increases monotonically as π increases; see an example in Fig. 7(a). This phenomenon was reported in Ref. [52] and it is now well understood.

We know that the faster information transmission is equivalent to the slower disease spreading. Since both the suppression effect and the promotion effect follow *image 2*, the information prevalence ρ_A will decrease as $1 - \pi$ decreases (or π increases). However, due to the presence of self-awareness, ρ_A will increase as ρ_I increases. Therefore, there are two competing physical mechanisms as π increases and it can be predicted that ρ_A will show different phenomena as the parameters change. For example, Fig. 7(b) shows that the curve ρ_A changes from monotonically increasing to almost constant and finally to monotonically decreasing as η increases.

V. CONCLUSION

In summary, we unravel the mystery of the relative timescales in the coevolution dynamics on multiplex networks through the analysis of physical images that are asymmetric external inputs, discretization of low rate region, and secondary outbreak. In particular, we have completely solved the barrier to understanding the phenomenon that the

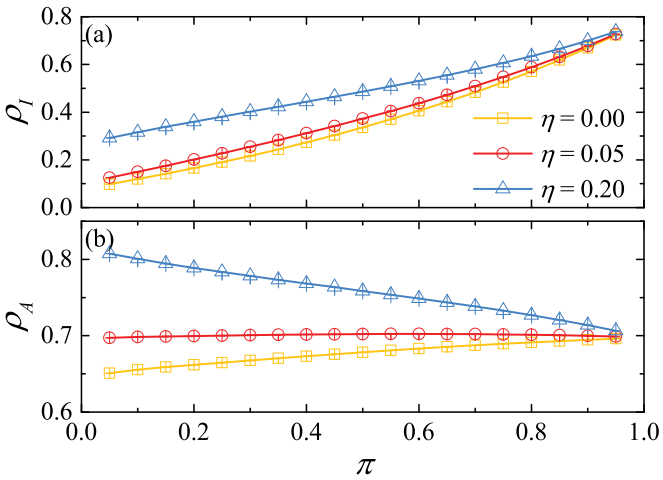

FIG. 7. Epidemic prevalence ρ_I and information prevalence ρ_A as a function of the relative timescales π in (a) and (b), respectively. The simulation results are obtained by averaging over 100 independent runs. The network is the same as in Fig. 5. Parameters: $\beta = 0.5$, $\mu = 1.0$, $\alpha = 0.0$, $\delta = 0.6$, $\kappa = 5.0$, $\rho_A(0) = 0.5$, and $\rho_I(0) = 0.01$.

prevalence of epidemics increases with the speed of information processing. We rely on information epidemic dynamics for the analysis and description and, in fact, these physical images are also applicable to other coevolution dynamics.

The physical image of discretization of the low rate region is based on the fact that, as the relative timescale increases, the state of the information layer changes more rapidly, resulting in the dispersion of the suppression effect in the epidemic layer. In the pioneering way of thinking, we found that the reason this property makes it easier for the disease to spread is that it reduces the average time required per unit rate, while not changing the average rate per unit time. This physical image applies to both irreversible and cyclic dynamics.

The physical image of asymmetric external inputs is based on the property that the information layer reaches the steady state faster as the relative timescales increase. Due to the asymmetry of the intensity of intralayer spreading and external inputs, this property can accelerate the consumption of external inputs or accelerate the growth of the intralayer itself. For cyclic dynamics, when the external input is multiplied by the same factor as the propagation intensity within the layer, we do not need to consider the influence of the external asymmetric input, such as the UAU-SIS model.

The physical image of the secondary outbreak is unique to irreversible dynamics, which is based on the fact that the effective reproduction number increases again due to some factors in the process of decreasing.

For the UAU-SIR model, asymmetric external inputs can produce a monotonically increasing or decreasing curve with different parameters, while discretization of the low rate region will only produce a monotonically increasing curve. With the competition between asymmetric external inputs and discretization of the low rate region, dominance may shift several times as the relative timescale increases. Specifically, as the relative timescale increases, the increase (slope) of the effect of discretization gradually decreases and the effect of external input asymmetry will reach saturation when the relative timescale is relatively large. In addition, there are two necessary conditions for a secondary outbreak: Sufficient remaining susceptible individuals and an increase in the effective reproduction number. Therefore, the curves of the final epidemic size $\rho_R(\pi)$ show five types of behavior, which are monotonically increasing, monotonically decreasing, first decreasing and then increasing, first increasing and then decreasing but increasing again, and suddenly increasing with large fluctuations. Moreover, with the increase of some parameters, the behavior of the curve will undergo qualitative changes several times. Although the phenomena are so complex, the physical images we present can fully explain them.

As an extension, our physical image of discretization of the low rate region can easily explain the phenomenon of monotonically increasing epidemic prevalence with increasing relative timescales in the UAU-SIS model. In addition, we also predict that the information prevalence shows different phenomena with the change of parameters, such as monotonically increasing and monotonically decreasing.

Finally, some remarks should be noted. (i) Although the UAU-SIS model mentioned in this paper does not include the physical image of asymmetric external inputs, the cyclic dynamics still needs to use this physical image when the external parameters do not agree with the amplification coefficients of the interlayer parameters. (ii) Although the physical image of discretization of the low rate region is used in this paper to study the timescale problem, it can also be used to analyze the amplification of some parameters or even the increase in the number of compartments. (iii) Secondary outbreaks can occur as long as two necessary conditions are met, which is not limited to the study in this paper.

In the future, on the one hand, we can consider applying our physical images to a broader range of coevolutionary dynamics, such as the coevolutionary game [57,58]. On the other hand, the heterogeneity of network structure, time-varying property [59], and higher order interaction [48] are also worthy of further study.

ACKNOWLEDGMENT

This work was supported by the Shaanxi Fundamental Science Research Project for Mathematics and Physics (Grant No. 22JSQ003).

APPENDIX A: PARTIAL EFFECTIVE DEGREE THEORY

We extend the partial effective degree theory [60] to the UAU-SIR model. Here, individuals are classified as U_kS_{si}, U_kI_{si}, A_kS_{si}, A_kI_{si}, U_kR, and A_kR. The subscript k represents the degree of the information layer and the subscripts s and i represent the number of susceptible neighbors and infected neighbors in the epidemic layer, respectively. Recovered individuals play no further role in the epidemic layer, so we do not need to track their numbers [61,62]. As a result, the value of the subscript $s + i$ decreases as infected neighbors recover, which is the difference from the UAU-SIS model.

For an individual, we should consider not only the change of its information layer state and epidemic layer state, but also the change of its epidemic layer subscripts. The dynamic

equations of the UAU-SIR model are as follows:

$$\begin{aligned}
\frac{dU_kS_{si}}{dt} &= -U_kS_{si}[\beta(1-\pi)i+\alpha\pi k\phi+\mu(1-\pi)i+Gs] \\
&\quad +A_kS_{si}\delta\pi+U_kS_{s+1,i-1}G(s+1) \\
&\quad +U_kS_{s,i+1}\mu(1-\pi)(i+1), \\
\frac{dU_kI_{si}}{dt} &= -U_kI_{si}[\mu(1-\pi)(1+i)+\alpha\pi k\phi+\kappa\pi+Hs] \\
&\quad +U_kS_{si}\beta(1-\pi)i+U_kI_{s+1,i-1}H(s+1) \\
&\quad +A_kI_{si}\delta\pi+U_kI_{s,i+1}\mu(1-\pi)(i+1), \\
\frac{dA_kS_{si}}{dt} &= -A_kS_{si}[\beta\eta(1-\pi)i+\delta\pi+\mu(1-\pi)i+Gs] \\
&\quad +U_kS_{si}\alpha\pi k\phi+A_kS_{s+1,i-1}G(s+1) \\
&\quad +A_kS_{s,i+1}\mu(1-\pi)(i+1), \\
\frac{dA_kI_{si}}{dt} &= U_kI_{si}(\alpha\pi k\phi+\kappa\pi)+A_kS_{si}\eta\beta(1-\pi)i \\
&\quad -A_kI_{si}[\mu(1-\pi)+\delta\pi+\mu(1-\pi)i+Hs] \\
&\quad +A_kI_{s+1,i-1}H(s+1)+A_kI_{s,i+1}\mu(1-\pi)(i+1), \\
\frac{dU_kR}{dt} &= -U_kR\alpha\pi k\phi+A_kR\delta\pi+\sum_{s,i}U_kI_{si}\mu(1-\pi), \\
\frac{dA_kR}{dt} &= U_kR\alpha\pi k\phi-A_kR\delta\pi+\sum_{s,i}A_kI_{si}\mu(1-\pi), \qquad \text{(A1)}
\end{aligned}$$

where G and H are the rates that a susceptible neighbor of susceptible individuals and infected individuals becomes an infected neighbor and ϕ is the rate of an unaware individual in contact with any aware individual. Their values can be approximated using the mean field method,

$$\begin{aligned}
G &= \frac{\sum_{k,s,i}[(U_kS_{si}+A_kS_{si}\eta)\beta(1-\pi)is]}{\sum_{k,s,i}[(U_kS_{si}+A_kS_{si})s]}, \\
H &= \frac{\sum_{k,s,i}[(U_kS_{si}+A_kS_{si}\eta)\beta(1-\pi)i^2]}{\sum_{k,s,i}[(U_kS_{si}+A_kS_{si})i]}, \\
\phi &= \frac{1}{\langle k\rangle}\sum_k\left\{k\left[A_kR+\sum_{s,i}(A_kS_{si}+A_kI_{si})\right]\right\}.
\end{aligned}$$

Finally, the final epidemic size ρ_R can be obtained by

$$\rho_R=\sum_k[U_kR(t=\infty)+A_kR(t=\infty)]. \qquad \text{(A2)}$$

In Sec. IV, we show that the numerical solutions of the partial effective degree theory are consistent with the Monte Carlo simulation results, which further proves the reliability of the simulation results.

APPENDIX B: SIMULATION PROCEDURE FOR THE UAU-SIR MODEL

The UAU-SIR model on multiplex networks can be simulated as follows.

Step 1. We build four lists b, c, d, and e for aware, unaware, infected, and susceptible nodes. We store the number of infected neighbors and aware neighbors for all nodes. We calculate B, C, D, and E as the transformation rates of $A \to U$, $U \to A$, $I \to R$, and $S \to I$.

Step 2. The total transition rate is $W = B + C + D + E$. There are four possible events. (1) With probability $\frac{B}{W}$, an aware node is chosen with equal probability from list b and becomes an unaware node. (2) With probability $\frac{C}{W}$, an unaware node is chosen from list c at random and accepted with probability $\frac{u}{u_{\max}}$, which is repeated until one choice is accepted. Here, u is the rate of $U \to A$ of the selected node and $u_{\max}$ is the maximum that u can possibly take. The accepted node becomes the aware node. (3)With probability $\frac{D}{W}$, an infected node is chosen with equal probability from list d and recovered. (4) With probability $\frac{E}{W}$, a susceptible node is chosen from list e at random and accepted with probability $\frac{n}{n_{\max}}$, which is repeated until one choice is accepted. Here, n is the rate of $S \to I$ of the selected node and $n_{\max}$ is the maximum that n can possibly take. The accepted node becomes the infected node.

Step 3. Update the time and all the quantities mentioned in Step 1, then go to Step 2 until there are no infected individuals left in the system.

In Step 2, we used the rejection method [63], which is usually more effective than the roulette method. The update in Step 3 requires simply updating any changes in the environment.

APPENDIX C: ANALYTIC CALCULATION OF ρ_A

To facilitate readers to compare the values of ρ_A and $\rho_A(0)$ when $\kappa = 0$, we give an analytic method for ρ_A by using the HMF-DC theory proposed in Ref. [64]. The process is as follows. (i) Calculate p from

$$\sum_k\left\{\frac{\lambda kpNP(k)}{1+\lambda kp}[(1-p)\lambda(k-1)-1]\right\}=0, \qquad \text{(C1)}$$

where $\lambda = \frac{\alpha}{\delta}$ and $P(k)$ is the degree distribution of the information layer. (ii) Substitute the value of p into

$$A_k=\frac{\lambda kp}{1+\lambda kp}NP(k) \qquad \text{(C2)}$$

to solve A_k. (iii) Obtain the required ρ_A by $\rho_A = \frac{1}{N}\sum_k A_k$. Here, p is the probability of reaching an arbitrary aware individual by following a randomly chosen edge from an unaware individual, A_k is the number of aware individuals with degree k, $P(k)$ is the degree distribution of an information layer, and $\lambda = \alpha/\delta$.

As an example, when $\alpha = 0.1$ and $\delta = 0.6$, ρ_A is about 0.377.

[1] A. Barrat, M. Barthélemy, and A. Vespignani, *Dynamical Processes on Complex Networks* (Cambridge University Press, Cambridge, UK, 2008).

[2] R. Pastor-Satorras, C. Castellano, P. Van Mieghem, and A. Vespignani, Epidemic processes in complex networks, Rev. Mod. Phys. **87**, 925 (2015).

[3] Z. Wang, C. T. Bauch, S. Bhattacharyya, A. d'Onofrio, P. Manfredi, M. Perc, N. Perra, M. Salathé, and D. Zhao, Statistical physics of vaccination, Phys. Rep. **664**, 1 (2016).

[4] I. Z. Kiss, J. C. Miller, and P. L. Simon, *Mathematics of Epidemics on Networks* (Springer, Heidelberg, 2017).

[5] W. Wang, M. Tang, H. E. Stanley, and L. A. Braunstein, Unification of theoretical approaches for epidemic spreading on complex networks, Rep. Prog. Phys. **80**, 036603 (2017).

[6] M. Gosak, M. Duh, R. Markovič, and M. Perc, Community lockdowns in social networks hardly mitigate epidemic spreading, New J. Phys. **23**, 043039 (2021).

[7] P. Ji, J. Ye, Y. Mu, W. Lin, Y. Tian, C. Hens, M. Perc, Y. Tang, J. Sun, and J. Kurths, Signal propagation in complex networks, Phys. Rep. **1017**, 1 (2023).

[8] Z. Wang, M. A. Andrews, Z.-X. Wu, L. Wang, and C. T. Bauch, Coupled disease-behavior dynamics on complex networks: A review, Phys. Life Rev. **15**, 1 (2015).

[9] V. Nicosia, P. S. Skardal, A. Arenas, and V. Latora, Collective Phenomena Emerging from the Interactions Between Dynamical Processes in Multiplex Networks, Phys. Rev. Lett. **118**, 138302 (2017).

[10] W. Wang, Q.-H. Liu, J. Liang, Y. Hu, and T. Zhou, Coevolution spreading in complex networks, Phys. Rep. **820**, 1 (2019).

[11] M. M. Danziger, I. Bonamassa, S. Boccaletti, and S. Havlin, Dynamic interdependence and competition in multilayer networks, Nat. Phys. **15**, 178 (2019).

[12] P. Bródka, K. Musial, and J. Jankowski, Interacting spreading processes in multilayer networks: A systematic review, IEEE Access **8**, 10316 (2020).

[13] H. Sun, D. Saad, and A. Y. Lokhov, Competition, Collaboration, and Optimization in Multiple Interacting Spreading Processes, Phys. Rev. X **11**, 011048 (2021).

[14] X. Wang, X. Zhu, X. Tao, J. Xiao, W. Wang, and Y.-C. Lai, Anomalous role of information diffusion in epidemic spreading, Phys. Rev. Res. **3**, 013157 (2021).

[15] B. Karrer and M. E. J. Newman, Competing epidemics on complex networks, Phys. Rev. E **84**, 036106 (2011).

[16] J. Sanz, C.-Y. Xia, S. Meloni, and Y. Moreno, Dynamics of Interacting Diseases, Phys. Rev. X **4**, 041005 (2014).

[17] W. Cai, L. Chen, F. Ghanbarnejad, and P. Grassberger, Avalanche outbreaks emerging in cooperative contagions, Nat. Phys. **11**, 936 (2015).

[18] L. Chen, F. Ghanbarnejad, and D. Brockmann, Fundamental properties of cooperative contagion processes, New J. Phys. **19**, 103041 (2017).

[19] G. F. de Arruda, E. Cozzo, T. P. Peixoto, F. A. Rodrigues, and Y. Moreno, Disease Localization in Multilayer Networks, Phys. Rev. X **7**, 011014 (2017).

[20] P. C. Ventura, Y. Moreno, and F. A. Rodrigues, Role of time scale in the spreading of asymmetrically interacting diseases, Phys. Rev. Res. **3**, 013146 (2021).

[21] J. P. Rodríguez and V. M. Eguíluz, Coupling between infectious diseases leads to synchronization of their dynamics, Chaos **33**, 021103 (2023).

[22] C. Granell, S. Gómez, and A. Arenas, Dynamical Interplay Between Awareness and Epidemic Spreading in Multiplex Networks, Phys. Rev. Lett. **111**, 128701 (2013).

[23] C. Granell, S. Gómez, and A. Arenas, Competing spreading processes on multiplex networks: Awareness and epidemics, Phys. Rev. E **90**, 012808 (2014).

[24] H. Wang, C. Ma, H.-S. Chen, and H.-F. Zhang, Effects of asymptomatic infection and self-initiated awareness on the coupled disease-awareness dynamics in multiplex networks, Appl. Math. Comput. **400**, 126084 (2021).

[25] X. Chen, R. Wang, M. Tang, S. Cai, H. E. Stanley, and L. A. Braunstein, Suppressing epidemic spreading in multiplex networks with social-support, New J. Phys. **20**, 013007 (2018).

[26] X. Chen, T. Zhou, L. Feng, J. Liang, F. Liljeros, S. Havlin, and Y. Hu, Nontrivial resource requirement in the early stage for containment of epidemics, Phys. Rev. E **100**, 032310 (2019).

[27] P. Huang, X.-L. Chen, M. Tang, and S.-M. Cai, Coupled dynamic model of resource diffusion and epidemic spreading in time-varying multiplex networks, Complexity **2021**, 6629105 (2021).

[28] Q. Sun, Z. Wang, D. Zhao, C. Xia, and M. Perc, Diffusion of resources and their impact on epidemic spreading in multilayer networks with simplicial complexes, Chaos Solitons Fractals **164**, 112734 (2022).

[29] C. T. Bauch and A. P. Galvani, Social factors in epidemiology, Science **342**, 47 (2013).

[30] L. J. Abu-Raddad, P. Patnaik, and J. G. Kublin, Dual infection with HIV and malaria fuels the spread of both diseases in sub-Saharan Africa, Science **314**, 1603 (2006).

[31] S. Funk, E. Gilad, C. Watkins, and V. A. A. Jansen, The spread of awareness and its impact on epidemic outbreaks, Proc. Natl. Acad. Sci. USA **106**, 6872 (2009).

[32] M. E. J. Newman, Threshold Effects for Two Pathogens Spreading on a Network, Phys. Rev. Lett. **95**, 108701 (2005).

[33] P.-B. Cui, F. Colaiori, and C. Castellano, Mutually cooperative epidemics on power-law networks, Phys. Rev. E **96**, 022301 (2017).

[34] A. Khazaee and F. Ghanbarnejad, Effects of measures on phase transitions in two cooperative susceptible-infectious-recovered dynamics, Phys. Rev. E **105**, 034311 (2022).

[35] M. De Domenico, A. Solé-Ribalta, E. Cozzo, M. Kivelä, Y. Moreno, M. A. Porter, S. Gómez, and A. Arenas, Mathematical Formulation of Multilayer Networks, Phys. Rev. X **3**, 041022 (2013).

[36] M. Kivelä, A. Arenas, M. Barthelemy, J. P. Gleeson, Y. Moreno, and M. A. Porter, Multilayer networks, J. Complex Netw. **2**, 203 (2014).

[37] M. De Domenico, C. Granell, M. A. Porter, and A. Arenas, The physics of spreading processes in multilayer networks, Nat. Phys. **12**, 901 (2016).

[38] V. Nanumyan, C. Gote, and F. Schweitzer, Multilayer network approach to modeling authorship influence on citation dynamics in physics journals, Phys. Rev. E **102**, 032303 (2020).

[39] Y. Guo, L. Tu, H. Shen, and L. Chai, Transmission dynamics of disease spreading in multilayer networks with mass media, Phys. Rev. E **106**, 034307 (2022).

[40] E. Massaro and F. Bagnoli, Epidemic spreading and risk perception in multiplex networks: A self-organized percolation method, Phys. Rev. E **90**, 052817 (2014).

[41] A. Hackett, D. Cellai, S. Gómez, A. Arenas, and J. P. Gleeson, Bond Percolation on Multiplex Networks, Phys. Rev. X **6**, 021002 (2016).

[42] F. Radicchi and G. Bianconi, Redundant Interdependencies Boost the Robustness of Multiplex Networks, Phys. Rev. X **7**, 011013 (2017).

[43] A. Tejedor, A. Longjas, E. Foufoula-Georgiou, T. T. Georgiou, and Y. Moreno, Diffusion Dynamics and Optimal Coupling in Multiplex Networks with Directed Layers, Phys. Rev. X **8**, 031071 (2018).

[44] Y. Huang, M. Tang, Y. Zou, and J. Zhou, Hybrid phase transitions of spreading dynamics in multiplex networks, Chin. J. Phys. **56**, 1166 (2018).

[45] X. Chang, C.-R. Cai, J.-Q. Zhang, and C.-Y. Wang, Analytical solution of epidemic threshold for coupled information-epidemic dynamics on multiplex networks with alterable heterogeneity, Phys. Rev. E **104**, 044303 (2021).

[46] J. Fan, Q. Yin, C. Xia, and M. Perc, Epidemics on multilayer simplicial complexes, Proc. R. Soc. A **478**, 20220059 (2022).

[47] X. Chang, C.-R. Cai, C.-Y. Wang, X.-S. Liu, J.-Q. Zhang, K. Jin, and W.-L. Yang, Combined effect of simplicial complexes and interlayer interaction: An example of information-epidemic dynamics on multiplex networks, Phys. Rev. Res. **5**, 013196 (2023).

[48] L. Liu, M. Feng, C. Xia, D. Zhao, and M. Perc, Epidemic trajectories and awareness diffusion among unequals in simplicial complexes, Chaos Solitons Fractals **173**, 113657 (2023).

[49] W. Wang, Q.-H. Liu, S.-M. Cai, M. Tang, L. A. Braunstein, and H. E. Stanley, Suppressing disease spreading by using information diffusion on multiplex networks, Sci. Rep. **6**, 29259 (2016).

[50] H. Wang, C. Chen, B. Qu, D. Li, and S. Havlin, Epidemic mitigation via awareness propagation in communication networks: The role of time scales, New J. Phys. **19**, 073039 (2017).

[51] P. C. Ventura da Silva, F. Velásquez-Rojas, C. Connaughton, F. Vazquez, Y. Moreno, and F. A. Rodrigues, Epidemic spreading with awareness and different timescales in multiplex networks, Phys. Rev. E **100**, 032313 (2019).

[52] F. Velásquez-Rojas, P. C. Ventura, C. Connaughton, Y. Moreno, F. A. Rodrigues, and F. Vazquez, Disease and information spreading at different speeds in multiplex networks, Phys. Rev. E **102**, 022312 (2020).

[53] H. Wang, H.-F. Zhang, P.-C. Zhu, and C. Ma, Interplay of simplicial awareness contagion and epidemic spreading on time-varying multiplex networks, Chaos **32**, 083110 (2022).

[54] Q. Yin, Z. Wang, and C. Xia, Information-epidemic coevolution propagation under policy intervention in multiplex networks, Nonlinear Dyn. **111**, 14583 (2023).

[55] R. M. Anderson and R. M. May, *Infectious Diseases of Humans: Dynamics and Control* (Oxford University Press, Oxford, 1991).

[56] In fact, for $\rho_A(0) = 0.1$, ρ_R increases by 0.002 when π increases from 0 to 0.05. We do not consider here changes that are so small that they are undetectable to the naked eye and are likely to disappear when the network structure is replaced.

[57] M. Perc and A. Szolnoki, Coevolutionary games–A mini review, Biosystems **99**, 109 (2010).

[58] Z. Wang, A. Szolnoki, and M. Perc, Self-organization towards optimally interdependent networks by means of coevolution, New J. Phys. **16**, 033041 (2014).

[59] D. Ghosh, M. Frasca, A. Rizzo, S. Majhi, S. Rakshit, K. Alfaro-Bittner, and S. Boccaletti, The synchronized dynamics of time-varying networks, Phys. Rep. **949**, 1 (2022).

[60] Y. Zhou, J. Zhou, G. Chen, and H. E. Stanley, Effective degree theory for awareness and epidemic spreading on multiplex networks, New J. Phys. **21**, 035002 (2019).

[61] J. Lindquist, J. Ma, P. van den Driessche, and F. H. Willeboordse, Effective degree network disease models, J. Math. Biol. **62**, 143 (2011).

[62] C.-R. Cai, Z.-X. Wu, and J.-Y. Guan, Effective degree Markov-chain approach for discrete-time epidemic processes on uncorrelated networks, Phys. Rev. E **90**, 052803 (2014).

[63] W. Cota and S. C. Ferreira, Optimized gillespie algorithms for the simulation of markovian epidemic processes on large and heterogeneous networks, Comput. Phys. Commun. **219**, 303 (2017).

[64] C.-R. Cai, Z.-X. Wu, M. Z. Q. Chen, P. Holme, and J.-Y. Guan, Solving the Dynamic Correlation Problem of the Susceptible-Infected-Susceptible Model on Networks, Phys. Rev. Lett. **116**, 258301 (2016).